

Conditional Normalizing Flows for Forward and Backward Joint State and Parameter Estimation

Luke S. Lagunowich¹, Guoxiang Grayson Tong², Daniele E. Schiavazzi³

¹Department of Computer Science and Engineering
University of Notre Dame, Notre Dame, IN, 46556, USA

²Department of Pediatrics
Stanford University, Stanford, CA, 94305, USA

³Department of Applied and Computational Mathematics and Statistics
University of Notre Dame, Notre Dame, IN, 46556, USA

Abstract

Traditional filtering algorithms for state estimation – such as classical Kalman filtering, unscented Kalman filtering, and particle filters – show performance degradation when applied to nonlinear systems whose uncertainty follows arbitrary non-Gaussian, and potentially multi-modal distributions. This study reviews recent approaches to state estimation via nonlinear filtering based on conditional normalizing flows, where the conditional embedding is generated by standard MLP architectures, transformers or selective state-space models (like Mamba-SSM). In addition, we test the effectiveness of an optimal-transport-inspired kinetic loss term in mitigating overparameterization in flows consisting of a large collection of transformations. We investigate the performance of these approaches on applications relevant to autonomous driving and patient population dynamics, paying special attention to how they handle time inversion and chained predictions. Finally, we assess the performance of various conditioning strategies for an application to real-world COVID-19 joint SIR system forecasting and parameter estimation.

1 Introduction

State estimation is an important task in a variety of scientific disciplines. In robotics, autonomous vehicles estimate their state from sensor measurements, which are often stochastic, resulting in uncertainty about the true underlying state. Similarly, in epidemiology, health agencies can infer the dynamics of underlying disease progression from uncertain diagnostic measurements, such as positive test cases. In essence, state estimation refers to the ability to infer the distribution of a d -dimensional state vector $\mathbf{x}_n \in \mathbb{R}^d$ at discrete times $t = n\Delta t$ with $n \in \{0, 1, \dots, N\}$, given the R observations $\{\mathbf{o}_{n-R}, \mathbf{o}_{n-R+1}, \dots, \mathbf{o}_{n-1}\}$, where $\mathbf{o}_{n-r} \in \mathbb{R}^m$, for $r = 0, \dots, R\Delta t$. Similarly, state estimation can be reversed, focusing on inference of a past state from future observations, or inferring \mathbf{x}_n given the R observations $\{\mathbf{o}_{n+1}, \mathbf{o}_{n+2}, \dots, \mathbf{o}_{n+R}\}$. This can be useful for capturing the dynamics of a system given an incomplete set of past or future observations in time. Additionally, while realistic decision-making processes – such as those in autonomous driving or epidemiological forecasting – often involve equally probable alternatives, classical state estimation techniques frequently struggle to capture complex multimodal distributions.

Classical state estimation methods like Kalman Filter [1] typically show performance degradation when applied to nonlinear systems and arbitrarily distributed non-Gaussian noise. To overcome these issues, a number of improvements were suggested. The Unscented Kalman Filter (UKF [2]), is designed to accommodate nonlinear models, but may fail to converge when a distribution contains uncertainty [3]. Similarly, particle filters are popular for their ability to handle nonlinear and non-Gaussian systems. However, it has been shown that traditional particle filters fail to converge when applied to high-dimensional and multi-modal data [4, 5].

Recent developments combining density estimation and deep neural networks have offered new possibilities for estimating non-Gaussian distributions for the states or parameters of nonlinear models. One class of such models are Mixture Density Networks (MDNs [6]) which parametrize the linear combination of Gaussian kernel functions. MDNs have been applied in trajectory modeling [7] and in rider demand forecasting as part of a novel recurrent architecture [8]. However, despite their increased performance with nonlinear systems, in their basic form MDNs struggle with multi-modal, non-Gaussian target distributions as discussed in [9]. Generative Adversarial Networks (GANs [10]) are a class of generative models that imitate complex distributions. However, GANs do not provide direct access to the generator distribution, preventing this approach to be used for density estimation and uncertainty quantification. Variational Autoencoders (VAEs [11]) use an encoder-decoder structure to perform probabilistic generative modeling tasks by optimizing the encoding of a simple prior distribution to represent the posterior and estimating the decoding of such representation. VAEs have been used in applications of finance [12], speech processing [13], and bio-signal processing [14] for their strength in learning complex input distributions for these tasks.

In this study we instead focus on Normalizing Flows (NF), which generate expressive probability distributions by applying a series of parametrized transformations to a simple *base* density, for which samples can be easily generated. NF are traditionally used in density estimation and generative modeling [15], and have been used to model complex distributions in time-series and image modeling [15], image generation [16], noise modeling [17], and physics [18, 19, 20, 21, 22]. Most significant to our work is the paper developed by Delecki et al. [23] which combines transformers with conditional normalizing flows. We propose various normalizing flow architectures parametrized with transformer and selective state-space model-based conditioning operators. Note that recurrent conditioning operators can generate embedding from sequences of varying length, providing unparalleled flexibility for filtering problems with an arbitrary number of past or future observations. We aim to combine the flexibility of these conditioning mechanisms with the expressive power of normalizing flows in representing a large class of densities for state-only and joint parameter/state estimation under uncertainty.

The paper is organized as follows. In Section 2.1, we start by introducing two dynamical systems of interest with applications in autonomous driving and epidemiology. Section 2.2 introduces normalizing flow and conditional normalizing flow architectures. Various strategies to generate conditional embeddings are discussed in Section 2.3, focusing on transformers and selective state-space models. In Section 2.3.1 we also introduce a kinetic term in the loss function and assess its effectiveness on density estimation accuracy. Results in Section 3 show the performance of the proposed approaches on the two selected dynamical systems, including forecast with real data from the COVID-19 pandemic. A discussion with possible ideas for future work are finally provided in Section 4.

2 Methods

2.1 Dynamical Systems

To validate the proposed architectures, we introduce two dynamical systems in the next sections.

2.1.1 Autonomous Vehicle Dynamics with Random Switching

We first consider a discrete bimodal dynamical system given by a set of four difference equation with a random switch parameter, originally proposed in [23]. This model represents the motion of an autonomous vehicle, where the bimodal trajectory could result from sensor readings while traversing a roundabout or intersection or after a sudden change in trajectory. To simulate realistic sensor data, we add noise to the trajectory determined by the following equations of motion. Consider the two-dimensional trajectory of a vehicle with location at time t expressed by the pair (p_x^t, p_y^t) and heading angle θ^t , which is updated at every time step according to the equations

$$\begin{aligned} p_x^{t+1} &= p_x^t + \Delta t \cdot v^t \cdot \cos(\theta^t) \\ p_y^{t+1} &= p_y^t + \Delta t \cdot v^t \cdot \sin(\theta^t) \\ \theta^{t+1} &= \theta^t + \Delta t \cdot v^t \cdot \phi^t, \end{aligned} \tag{1}$$

where the angular acceleration ϕ^t at time t is updated with the formula

$$\phi^{t+1} = \phi^t + \Delta t \cdot \psi \cdot c_1 \cdot \cos(c_2 \cdot t). \quad (2)$$

The autonomous vehicle is nonholonomic and has control over its velocity v^t and angular acceleration ϕ^t . Uncertainty in vehicle position accumulates over time as Gaussian noise is added to v^t and ϕ^t with $\sigma_v = 0.01$ and $\sigma_\phi = 0.025$, respectively, at each time step. The quantities $c_1 = 0.1$ and $c_2 = 0.5$ are constants, and ψ is a random switching parameter which is drawn from a uniform distribution $\psi \sim U([-1, 1])$ at a fixed time index $t = 5.5$ in the trajectory. This parameter is used to introduce multimodality in the resulting trajectory. A fixed time step of $\Delta t = 0.1$ is selected. The dataset is shown in Figure 1 (left panel). The black line represents the nominal noiseless trajectory. As in [23], the dataset consists of approximately of 1.5 million data points.

2.1.2 Epidemiological Population Dynamics

As a second model, we consider a simple compartmental model to represent the susceptible, infectious, and removed, by death or by recovery, (S, I, and R) patient populations with applications to the epidemiology of an infectious disease. We purposefully omit general birth and death rates from our model, assuming the dynamics of an epidemic are much more rapid than the dynamics of birth and death. The SIR model can be represented by the following system of ordinary differential equations

$$\frac{dS}{dt} = \dot{S} = -\beta I S, \quad \frac{dI}{dt} = \dot{I} = \beta I S - \gamma I, \quad \frac{dR}{dt} = \dot{R} = \gamma I, \quad (3)$$

where S is the number of susceptible individuals, I the number of infected individuals, and R the number of removed (dead or recovered) individuals. In addition, β is the infection rate, and γ is the recovery rate. For the simulated model, we select the parameters $\beta = 0.03$ and $\gamma = 0.01$ to ensure the reproduction number, the number of new infected individuals an infected person can cause, $R_0 > 1$, yielding nontrivial epidemic dynamics over a moderate time horizon. The system is solved using the Fourth Order Runge-Kutta method. Noise with $\sigma = 0.001$ is used for the single trajectory system. The low magnitude is chosen to improve robustness without affecting the dynamics of the underlying system. Figure 1 (right panel) shows simulated noisy trajectory observations for each of the three sub-populations, where the black lines represent the nominal trajectories. Similar to the previous application, this dataset contains over 1.5 million data points.

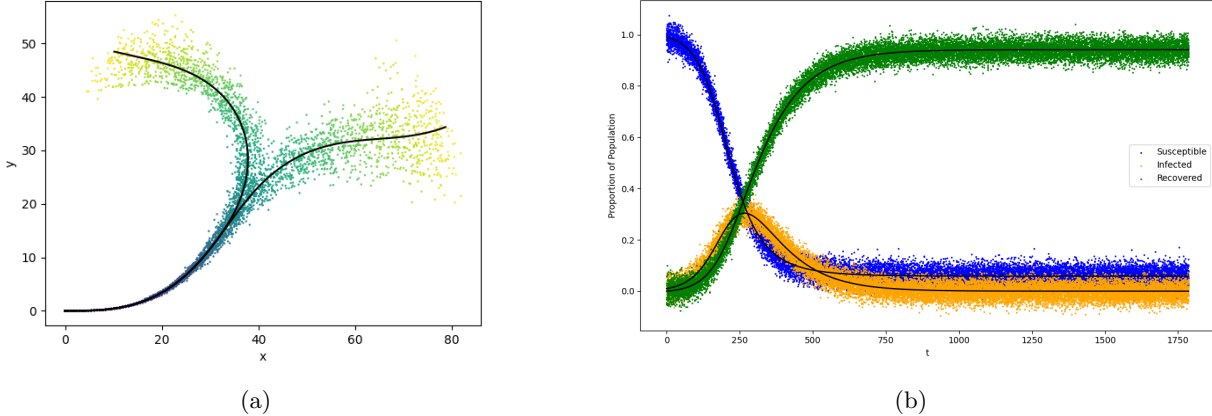


Figure 1: Sensor data for (a) autonomous vehicle with random switching, and (b) noisy trajectories from the dynamical epidemiological SIR model.

2.2 Conditional Density Estimation with Normalizing Flow

In this study, we explore state and parameter estimation using a normalizing flow-based architecture, where we assess the performance of various conditioning operators and loss function formulations.

A normalizing flow (NF) consists of a series of invertible mappings that characterize the transformation of a probability density. In more detail, a NF maps a simple *latent* distribution $p_{\mathbf{Z}}(\mathbf{z})$ to an arbitrary target density $p_{\mathbf{X}}(\mathbf{x})$ through a collection of invertible transformations via the change of variable formula

$$p_{\mathbf{X}}(\mathbf{x}) = p_{\mathbf{Z}}(f^{-1}(\mathbf{x})) \left| \det \left(\frac{df^{-1}(\mathbf{x})}{d\mathbf{x}} \right) \right|, \quad (4)$$

where $\mathbf{f}(\cdot, \boldsymbol{\theta}) = \mathbf{f}_1(\cdot, \boldsymbol{\theta}_1) \circ \mathbf{f}_2(\cdot, \boldsymbol{\theta}_2) \circ \dots \circ \mathbf{f}_L(\cdot, \boldsymbol{\theta}_L)$ is a composition of L smooth, invertible diffeomorphisms, and $\boldsymbol{\theta} = \{\boldsymbol{\theta}_1, \boldsymbol{\theta}_2, \dots, \boldsymbol{\theta}_L\}$. NF is a widely used machine learning paradigm for density estimation. Once trained, it allows for both the efficient generation of new samples and likelihood evaluation. This requires each transformation f_i , $i = 1, \dots, L$ to be easily invertible, and fast computation for the determinant of its Jacobian. Various formulations are proposed in the literature and the interested reader is referred to the two reviews in [24, 15] for additional details. For discrete NF, two widely popular approaches are based on transformations consisting of *affine couplings*, for example RealNVP [25], or *autoregressive transformations*, like masked autoregressive flows (MAF) introduced in [26]. We use MAF in all examples in this study. Because in practice an autoregressive flow depends on the order of input variables, it has been proven beneficial to permute inputs between layers [26]. Thus the resulting flow architecture consists of stacked layers containing a permutation, a linear layer, and a masked affine autoregressive flow.

Importantly, NF architectures can also be used to generate samples from or evaluate the likelihood of conditional distributions. In practice, conditioning is incorporated into both the base distribution and each MAF layer. A conditioned base distribution allows the latent variables \mathbf{Z} to depend on the context. Similarly, within each MAF layer, the input is augmented so that the transformation variables also depend on the context. We use the *nflows* Python library [27] throughout this study, where a *context* vector is injected into both the base distribution and each layer of the flow, consistent with the above discussion.

2.3 Generating Conditional Embeddings

We use normalizing flows to perform forward and inverse state estimation based on simulated observations from a dynamical system. For this task, we condition a normalizing flow on previous $\{\mathbf{o}_{n-R}, \mathbf{o}_{n-R+1}, \dots, \mathbf{o}_{n-1}\}$ and future $\{\mathbf{o}_{n+1}, \mathbf{o}_{n+2}, \dots, \mathbf{o}_{n+R}\}$ observations, taken from the noisy solutions of two dynamical systems. We then estimate the probability density of state \mathbf{x}_n , by approximating the probability distributions $p(\mathbf{x}_n | \mathbf{o}_{n-R}, \mathbf{o}_{n-R+1}, \dots, \mathbf{o}_{n-1})$ and $p(\mathbf{x}_n | \mathbf{o}_{n+1}, \mathbf{o}_{n+2}, \dots, \mathbf{o}_{n+R})$, i.e., conditioned on R past or future observations. Due to the sequential nature of time series data, we can utilize this conditioning operation recursively, estimating future state and then using these predicted states for conditioning, and so on and so forth. We call this paradigm *rollout*, which allows to estimate all future (past) states of the system from a limited number of observations.

We consider two approaches to generate meaningful conditional embeddings. First, we use a transformer network to condition the flow on the provided context. A schematic of this idea is shown in Figure 2a. We employ a model architecture like the one described in [28]. The model consists of encoder and decoder layers. The encoder is composed of an input layer, a positional encoding layer, and a stack of four identical encoder layers. Each encoder layer consists of two sub-layers: a self-attention sub-layer and a fully-connected feed-forward sub-layer. The decoder is composed of an input layer, four identical decoder layers, and an output layer. In addition to the two sub-layers in each encoder layer, the decoder inserts a third sub-layer to apply self-attention mechanisms over the encoder output. We employ a one-position offset and look-ahead masking to prevent look-ahead bias. Instead of using the transformer architecture for sequence-to-sequence forecasting, we use it to learn an embedding. Since there is no ground truth target sequence in this approach, we can freely choose the dimensionality of the embedding space without being constrained by the output sequence structure.

As an alternative to transformers, state space models (SSMs) can be used to process sequential information. SSMs represent the hidden or internal dynamics of a system through a set of first-order recurrence relations. At each time step, the hidden state evolves according to a linear *update* equation while outputs are generated through a *measurement* equation. Both equations are typically first-order differential equations. More specifically, the system of equations defines a map between inputs $\mathbf{x}(t)$ and outputs $\mathbf{y}(t)$ through a

hidden state $\mathbf{h}(t)$ through the equations

$$\begin{aligned}\mathbf{h}'(t) &= \mathbf{A} \mathbf{h}(t) + \mathbf{B} \mathbf{x}(t) \\ \mathbf{y}(t) &= \mathbf{C} \mathbf{h}(t),\end{aligned}\tag{5}$$

where \mathbf{A} , \mathbf{B} , \mathbf{C} are learnable matrices. \mathbf{A} is the state matrix, \mathbf{B} is the input or control matrix, and \mathbf{C} is the output matrix. The model is then computed in two stages. First, the continuous system parameters are converted to discrete parameters using *zero-order hold* (ZOH, see, e.g. [29]). Next, the model can be computed in two ways: linear recurrence or global convolution, each with implications in terms of both accuracy and efficient implementation. However, vanilla state space models are time invariant, meaning that \mathbf{A} , \mathbf{B} , \mathbf{C} are constant through time, instead of depending on the provided context. Improved expressiveness was introduced with selective state space models and the Mamba-SSM architecture, which removes linear time invariance, boosts parallel efficiency, and uses selection to improve input context awareness [30]. We leverage this architecture to condition the normalizing flow on past and future observations. The state space model context encoder maps the normalized output embedding of the Mamba-SSM to the desired dimensionality used in conditioning the normalizing flow. A diagram adapted from [30] is shown in Figure 2b.

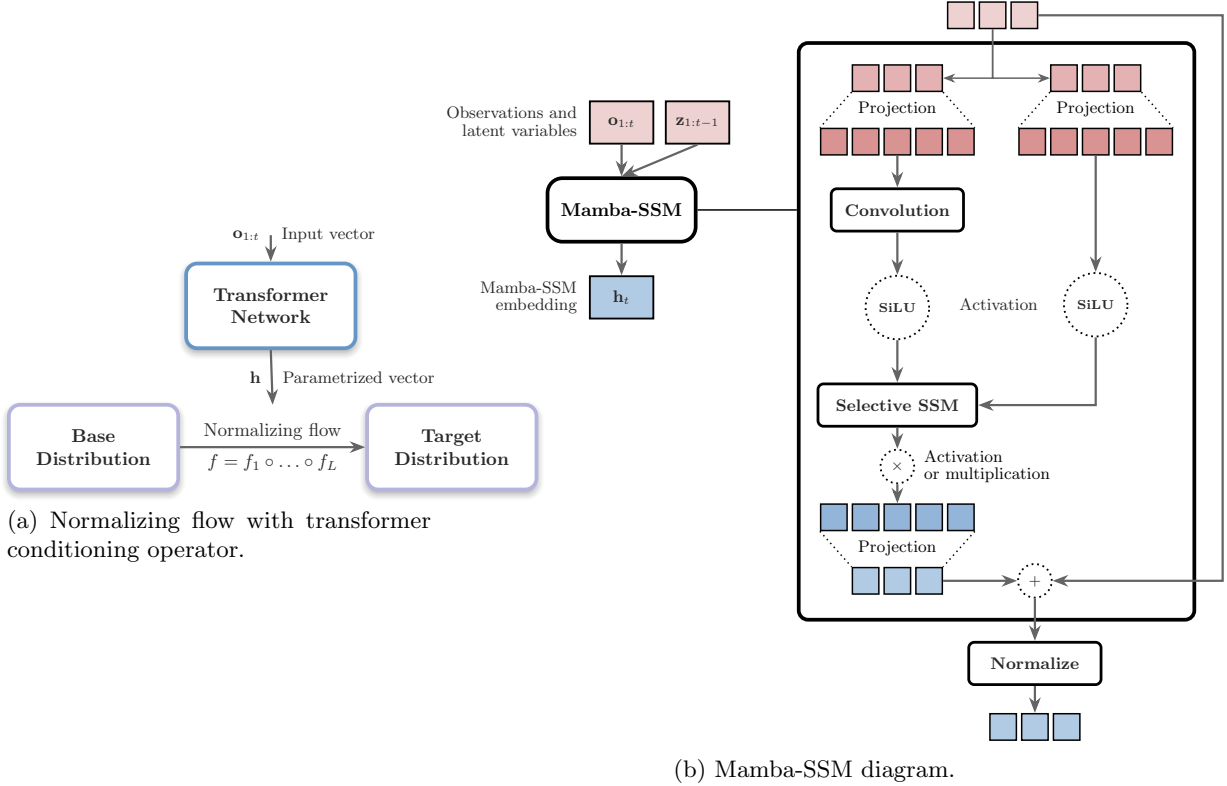


Figure 2: Generation of conditional embeddings using either a transformer or mamba-SSM architecture.

2.3.1 Optimal Transport-inspired Kinetic Term

Optimal transport provides a mathematical framework for finding the most efficient way to transform one probability distribution into another [31]. In this context, a normalizing flow can be understood as learning a map (realized through a composition of diffeomorphisms) $f: \mathbb{R}^d \rightarrow \mathbb{R}^d$ that transforms samples \mathbf{z} from the base distribution to samples \mathbf{x} from the target density. In other words, a NF defines a *path* between the base and target probability distribution. Paths associated with minimal Kinetic Energy (KE) lead to Optimal Transport (OT) interpolants, characterized by minimal Wasserstein distance with respect to the base and target densities. Additionally, since a NF architecture is typically overparameterized, regularization in terms of KE can mitigate the effects of overparameterization.

Therefore, inspired by recent research in optimal transport [31], we add a *kinetic energy* term to the loss function [32, 33]. Formally, we augment the standard maximum likelihood objective used in training normalizing flows with a kinetic regularization term and a layer-wise prior matching penalty

$$\begin{aligned} \inf_{\theta} \mathcal{L}(\theta) = & \lambda_1 \mathbb{E}_{\mathbf{x} \sim p_{\mathbf{X}}(\mathbf{x})} [-\log p_{\mathbf{X}}(\mathbf{x}; \theta)] + \lambda_2 \frac{1}{L-1} \sum_{\ell=1}^{L-1} \mathbb{E}_{\mathbf{x} \sim p_{\mathbf{X}}(\mathbf{x})} [\|f_{\ell+1}(\mathbf{x}) - f_{\ell}(\mathbf{x})\|_2] \\ & + \lambda_3 \frac{1}{L-1} \sum_{\ell=1}^{L-1} \mathbb{E}_{\mathbf{x} \sim p_{\mathbf{X}}(\mathbf{x})} [-\log p_{\mathbf{Z}}(f_{\ell}(\mathbf{x}))] \end{aligned} \quad (6)$$

where f_l , $l = 1, \dots, L$ are the members of the NF collection of transformations and λ_1 , λ_2 , and λ_3 are regularization penalties. In equation (6), the first term corresponds to the negative log-likelihood of the entire composition of transformations, whereas the second term acts as a kinetic regularizer, encouraging smooth transitions between consecutive flow layers. Finally, the third term maximizes the likelihood for intermediate layer outputs. For a preliminary assessment of the effects produced by KE regularization, we train an unconditional NF to estimate the well-known *double moon* distribution [34] with and without considering the KE term and report the results in Figure 3. As expected, KE regularization leads to smoother probability paths, minimizing sample movement between two successive normalizing flow layers.

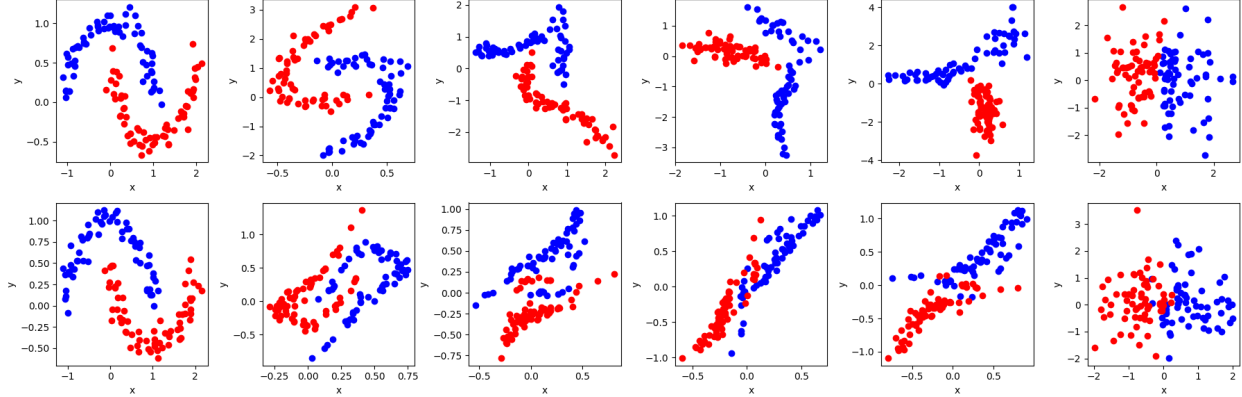


Figure 3: Unconditional normalizing flow transform trained without (top) and with (bottom) kinetic loss term. Each plot is obtained by extracting the distribution of the output of each layer in the forward mapping $f(\cdot, \theta)$ from the target density $p_{\mathbf{X}}(\mathbf{X})$ to the base distribution $p_{\mathbf{Z}}(\mathbf{Z})$. Note the effect of input parameter swap due to a permutation being performed between successive layers.

2.3.2 Evaluating Distances using Kullback–Leibler Divergence

To evaluate the performance of conditional NF in forward and backward state estimation, we perform repeated calculations of the Kullback–Leibler (KL) divergence between two distributions that are not necessarily evaluated over the same samples. While, in principle, one can use density estimation on both distributions and then evaluate them at a common set of samples, this will incur a significant computational cost. We instead use the following estimate suggested in [35, 23]. Given $\mathbf{z} \in \mathbb{R}^d$, n samples from $\hat{p}(\mathbf{z})$, and m samples from $p(\mathbf{z})$, one has

$$D_{KL}(\hat{p}(\mathbf{z}) \parallel p(\mathbf{z})) \approx \frac{d}{n} \sum_{i=1}^n \log \frac{r_k(\mathbf{z}^{(i)})}{s_k(\mathbf{z}^{(i)})} + \log \left(\frac{m}{n-1} \right), \quad (7)$$

where $r_k(\mathbf{z}^{(i)})$ and $s_k(\mathbf{z}^{(i)})$ are the Euclidean distance to the k -th nearest neighbor of $\mathbf{z}^{(i)}$ in the samples from $\hat{p}(\mathbf{z})$ and $p(\mathbf{z})$, respectively.

2.3.3 Training

We trained a normalizing flow with 10 layers, each containing an autoregressive transformation with 2 inputs, 4 hidden features, 4 context variables, with no batch normalization applied to the outputs. Also, a 2-layer MLP is used to encode the transformer or mamba-based embedding onto the parameters of the base distribution. Such embedding is created using five sequential observations in time, adding Gaussian noise with $\sigma = 1.0$. We perform 10,000 training iterations, using Adam a batch size of 2,048 and a constant learning rate equal to 0.001. Figure 4 shows a representative training loss profile for two conditioning operators (i.e., transformer- and mamba-based) as well as combining transformer conditioning plus KE loss augmentation for normalizing flow.

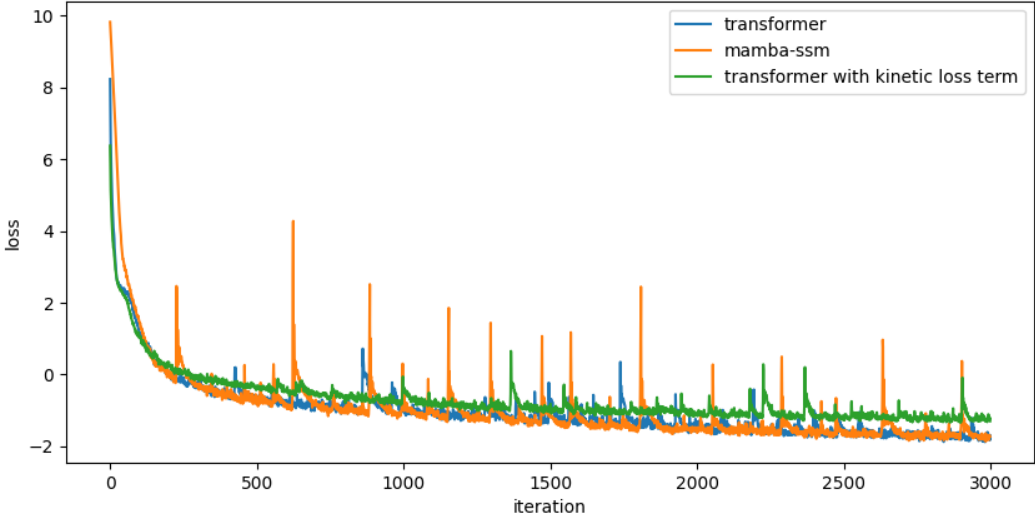


Figure 4: Example of training losses for different normalizing flow conditioning operators over 3,000 iterations.

3 Results

3.1 Autonomous Vehicle Dynamics with Random Switch

After training the conditional NFs, forward state estimation is performed by providing $R = 5$ previous noisy observations for the vehicle location as context, and estimating the conditional density for the next observation in sequence. In other words, assuming an initial observation at discrete time n , we estimate the density

$$p(\mathbf{x}_{n+5} | \mathbf{o}_n, \mathbf{o}_{n+1}, \dots, \mathbf{o}_{n+4}) \quad (8)$$

Similarly, for backward state estimation we provide $R = 5$ future noisy vehicle positions and estimate the density for the previous observation in the sequence, or

$$p(\mathbf{x}_{n-5} | \mathbf{o}_n, \mathbf{o}_{n-1}, \dots, \mathbf{o}_{n-4}) \quad (9)$$

We also evaluate the effectiveness of forward and backward state estimation for contexts that are provided at three different locations along the bimodal trajectory. Specifically, we consider contexts that include locations before the bifurcation, at the bifurcation, and after the bifurcation as shown in Figure 5, 6, and 7, respectively.

In addition, we calculate the KL divergence between 1,000 samples from the estimated conditional density and the true distributions of the \mathbf{x}_{n+5} and \mathbf{x}_{n-5} at the three locations along the trajectory. Aggregated

		Model		
		Transformer	Transformer + KE	Mamba-SSM
Sample	Before-bifurcation (fw)	3.654	3.264	3.716
	Before-bifurcation (bw)	3.163	2.78	3.263
	At-bifurcation (fw)	3.179	2.853	3.162
	At-bifurcation (bw)	3.279	2.83	3.354
	After-bifurcation (fw)	3.143	2.826	3.216
	After-bifurcation (bw)	3.318	2.903	3.361

Table 1: Mean KL divergence between 1,000 samples from estimated conditional density and true distribution when predicting next and previous states at three different locations along the vehicle trajectory.

results are shown in Table 1. As previously shown in Figure 3, the addition of the kinetic loss term results in smoother transformations from the base to the target distribution, leading to improve accuracy. Such configuration better captures the true conditional density without exhibiting bias towards a certain mean trajectory in the bifurcation, thus leading to a lower average KL-divergence aggregated over many noisy samples.

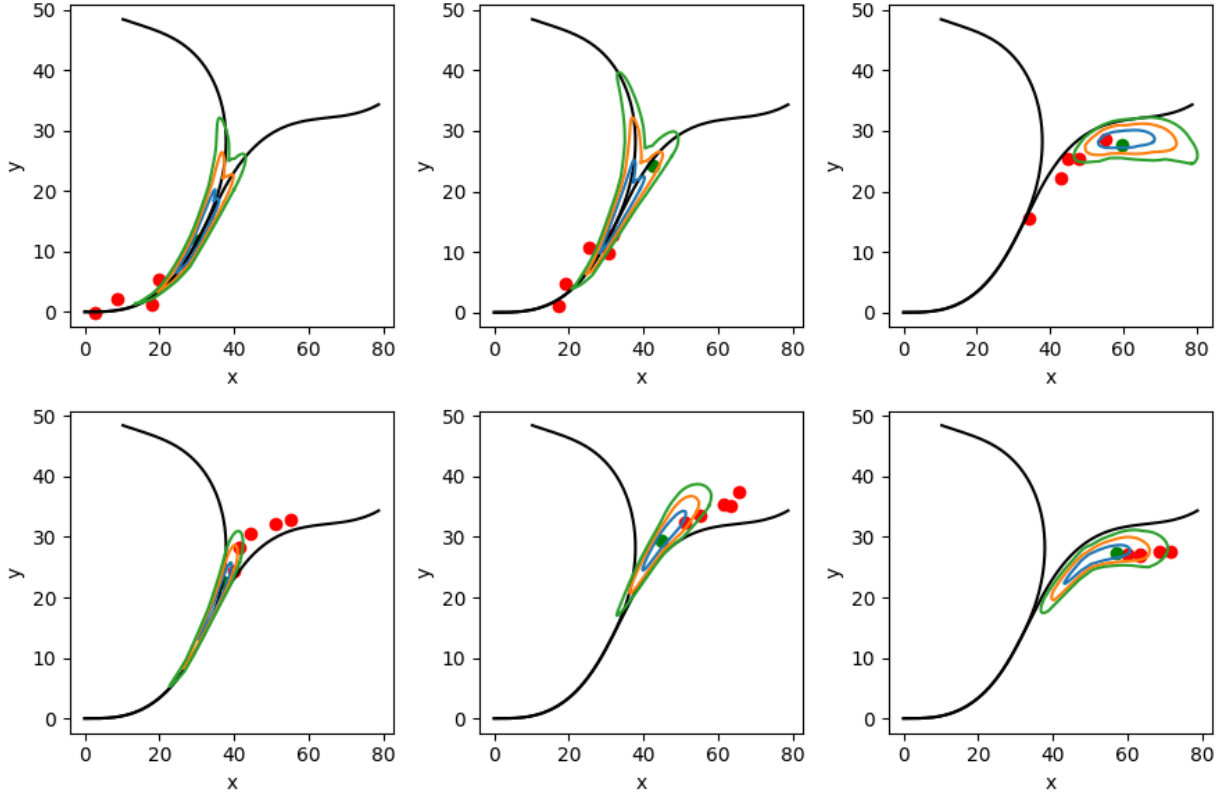


Figure 5: Confidence regions corresponding to 1, 2, and 3 base distribution standard deviations for forward (top) and backward (bottom) state estimation, for NF with transformer-based conditioning. Predicted density refers to three locations along the trajectory (left to right).

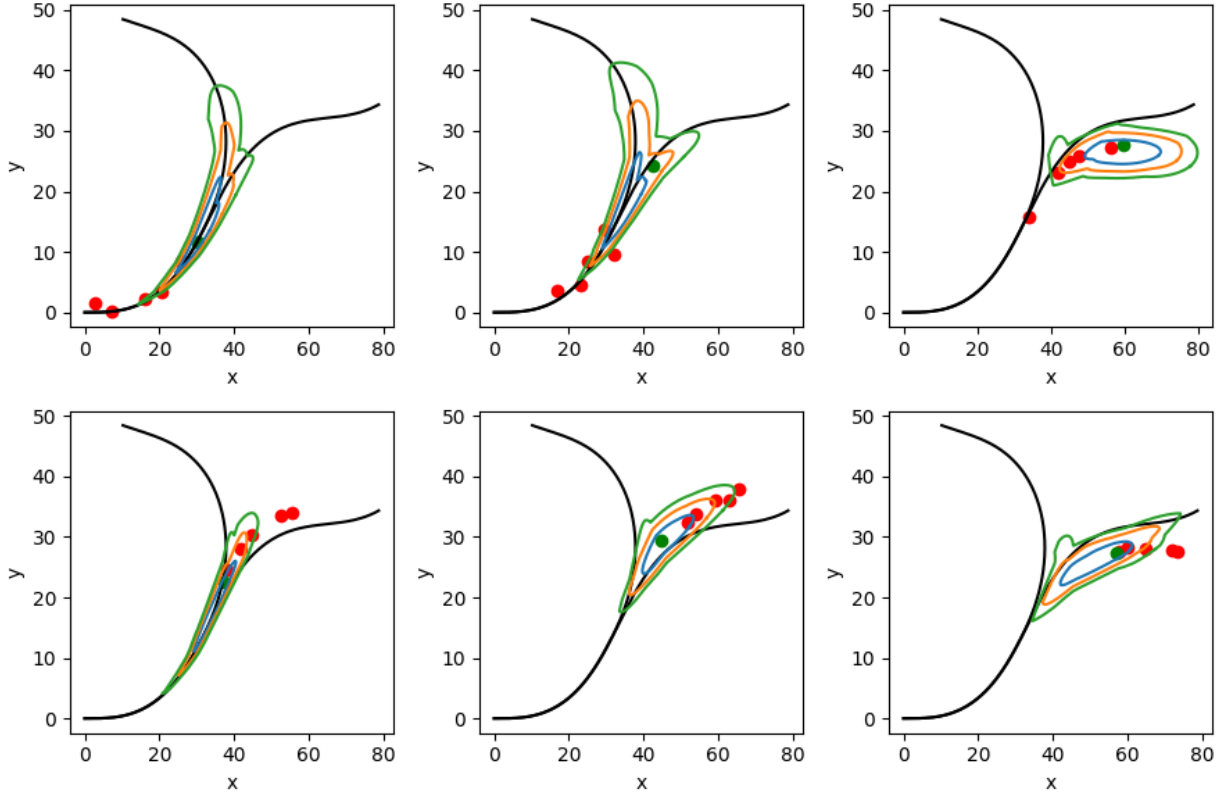


Figure 6: Confidence regions corresponding to 1, 2, and 3 base distribution standard deviations for forward (top) and backward (bottom) state estimation, for NF with transformer-based conditioning, plus KE loss term. Predicted density refers to three locations along the trajectory (left to right).

3.2 SIR Model

While the advantage of performing joint forward and backward conditional state estimation may not be readily apparent in the context of autonomous vehicles, it is certainly evident with epidemiological data. For applications in epidemiology, making past and future estimates for the number of susceptible, infected or recovered individuals from a snapshot of uncertain observations in time can lead to an improved understanding of disease progression dynamics. Also, estimates of the progression of the underlying system parameters are essential to inform public health policies.

In Figure 8 we visualize 1σ uncertainty regions for forward and backward state density estimation resulting from training using a single SIR model solution (one set of β , γ and initial conditions). We also compare the results for various conditioning operators. Furthermore, Table 2 shows the mean KL divergence between 1,000 samples from estimated conditional densities and the true underlying distributions at randomly chosen points along the SIR model trajectory. The results demonstrate that all conditional flows achieve a low KL divergence when applied to the SIR model compared to the multimodal autonomous driving dataset. Among the conditioning operators, Mamba-SSM achieves the lowest KL-divergence in the susceptible compartment for both forward and backwards state estimation. We attribute this performance to the temporal dependencies and unimodal nature of the SIR trajectories. Mamba’s selective state-space architecture is particularly well-suited to capture a trajectory governed by ODEs because it maintains a latent representation of the system, thus explaining its strong performance compared to the transformer architectures which rely more on local context. That said, the transformer architectures exhibit lower KL divergence in the infected and recovered compartments.

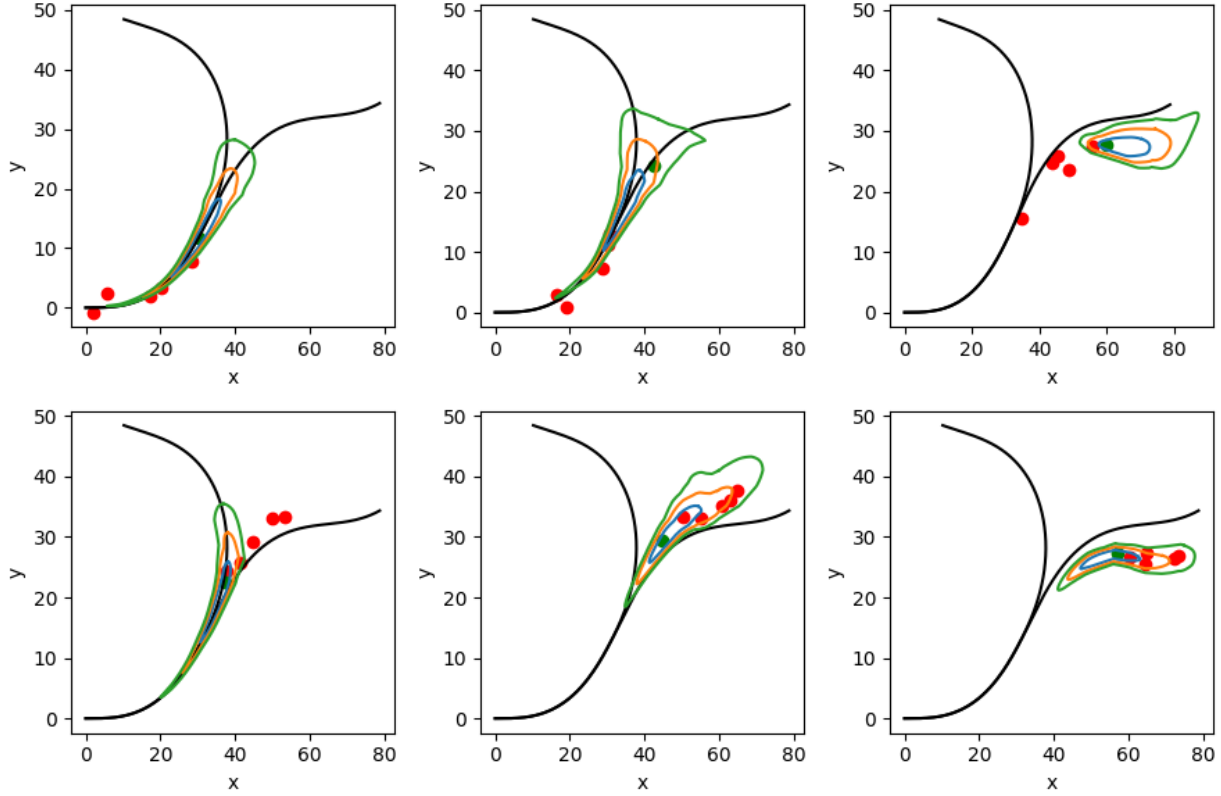


Figure 7: Confidence regions corresponding to 1, 2, and 3 base distribution standard deviations for forward (top) and backward (bottom) state estimation, for NF with Mamba-SSM-based conditioning. Predicted density refers to three locations along the trajectory (left to right).

		Model								
		Transformer			Transformer + KE			Mamba-SSM		
Sample	fw	S	I	R	S	I	R	S	I	R
	bw	4.357	4.972	4.104	4.447	4.923	4.159	4.331	4.951	4.138

Table 2: Mean KL divergence between 1,000 samples from the estimated conditional density and the true distribution for forward and backward state estimation at 100 randomly sampled locations along the noisy SIR trajectory. Errors are shown separately for each compartment S , I , and R .

3.2.1 Training with Multiple Trajectories

After assessing the ability of conditional NF to accurately infer states from a single SIR trajectory, we study the ability of the system to work with multiple trajectories using the data set shown in Figure 9. The data set shows noisy susceptible, infected, recovered populations as a proportion of the total population over time.

Figure 10 shows the ability of NF in forward and backward state estimation given a noisy context from a single SIR model solution but trained on multiple trajectories. We observe that the model is able to

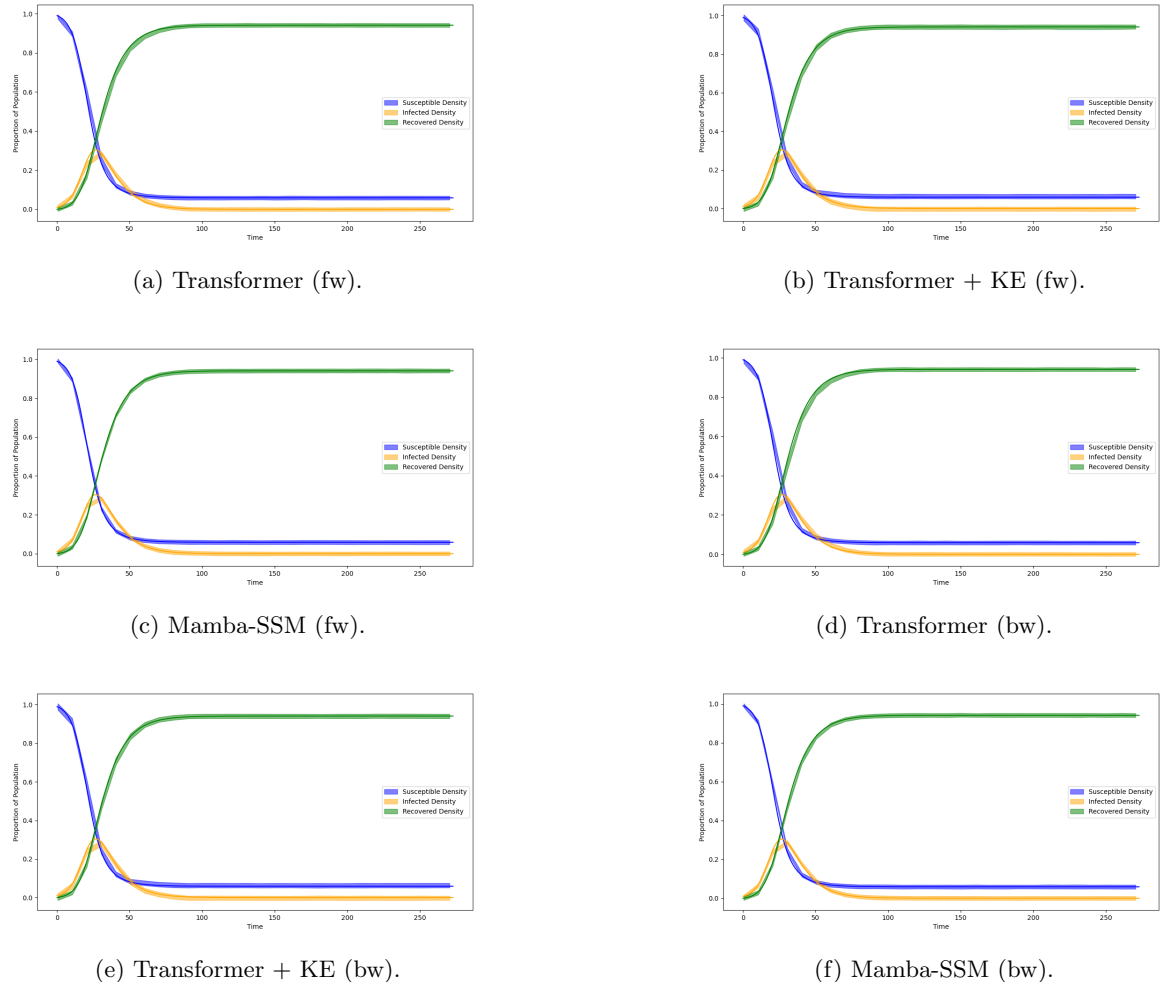


Figure 8: Comparison of 1σ error bounds for forward (fw) and inverse (bw) state predictions given a five-step observation context at various points in the SIR system. (a,d) NF with transformer conditioning operator, (b,e) NF with transformer conditioning operator and kinetic energy (KE) loss, (c,f) NF with Mamba-SSM conditioning operator.

accurately predict the next state and correctly identify the singular underlying trajectory for the susceptible and recovered populations despite being trained on multiple trajectories. The infected portion of the population is predicted with relatively lower accuracy. This is likely due to its reduced sensitivity to changes in the underlying system parameters, having a negative effect on the generalization abilities of the proposed approach. Finally, Table 3 shows the resulting mean KL divergence for this case.

3.2.2 COVID-19 Dataset

To further test the ability of NF to predict future trends with real data when trained from synthetic model solutions, we present a real-world state estimation task using COVID-19 data collected by the City and County of San Francisco Department of Public Health. The dataset used for our analysis is available on DataSF, the Office of the Chief Data Officer [36]. Figure 11 shows the generated SIR data from case, testing, and death reports, obtained using a similar data transformation process as in [37].

First, we perform forward and backward state estimation using a context which consists of real COVID-19 SIR observations, using NF trained on synthetic SIR trajectories with parameters drawn as $\beta \sim \mathcal{U}[0.02, 0.04]$ and $\gamma \sim \mathcal{U}[0.005, 0.025]$ and initial conditions $S_0 = 0.99$, $I_0 = 0.01$, and $R_0 = 0.00$.

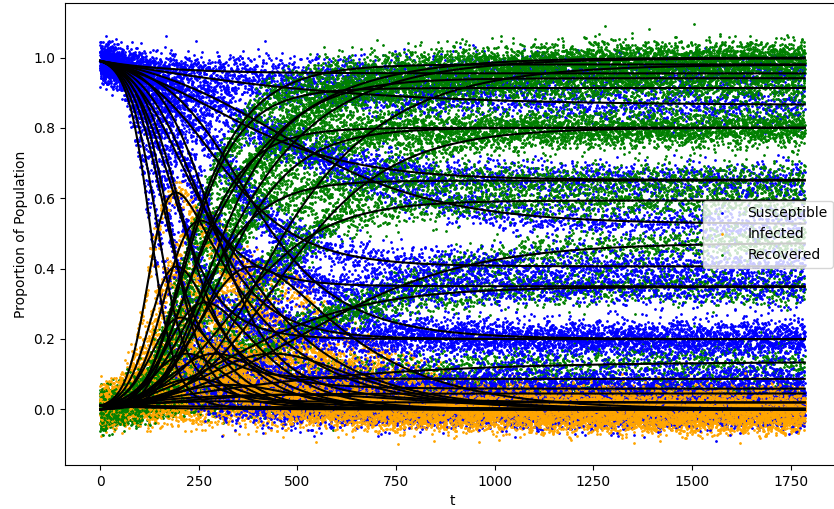


Figure 9: Ensemble of noisy SIR model solutions for dataset with multiple trajectories.

		Model								
		Transformer			Transformer + KE			Mamba-SSM		
Sample	S	I	R	S	I	R	S	I	R	
	fw	4.188	4.955	4.208	4.795	4.991	4.881	4.168	5.019	4.223
	bw	4.044	4.969	4.239	4.845	4.973	4.869	4.185	5.021	4.132

Table 3: Mean KL divergence between 1,000 samples from estimated conditional density and true distribution. Forward and backward state estimation is performed at 100 randomly sampled locations along the noisy SIR trajectory. The conditional NF predictor is trained on multiple SIR trajectories with various conditioning operators. Errors are shown separately for each compartment S , I , and R .

We then perform a forward and backward rollout exercise to test the ability of NF to predict future or past epidemiological trends. The results are reported in Figure 12 and Figure 13 with 2σ error. The results in the figure shows an ability of NF to predict future and past disease trends, particularly based on entirely synthetic knowledge. The mean negative log likelihood between the distributions of estimated and true states for the San Francisco COVID-19 test case is summarized in Table 4.

3.2.3 Predicting Disease System Parameters

An additional feature that complements state prediction, and is particularly useful for applications in epidemiology is the ability to simultaneously estimate meaningful system parameters. For the selected application, the transmission rate parameter β and the recovery rate parameter γ are key for domain experts to understand and classify the underlying disease and to inform public policy. The proposed NF approach, can be easily extended to explicitly estimate the joint density of the SIR states and parameters of the underlying system. An example of joint estimate of states and parameters for the San Francisco COVID-19 dataset is shown in Figure 14 which reports the estimated parameters, quantifies their uncertainty, and shows the

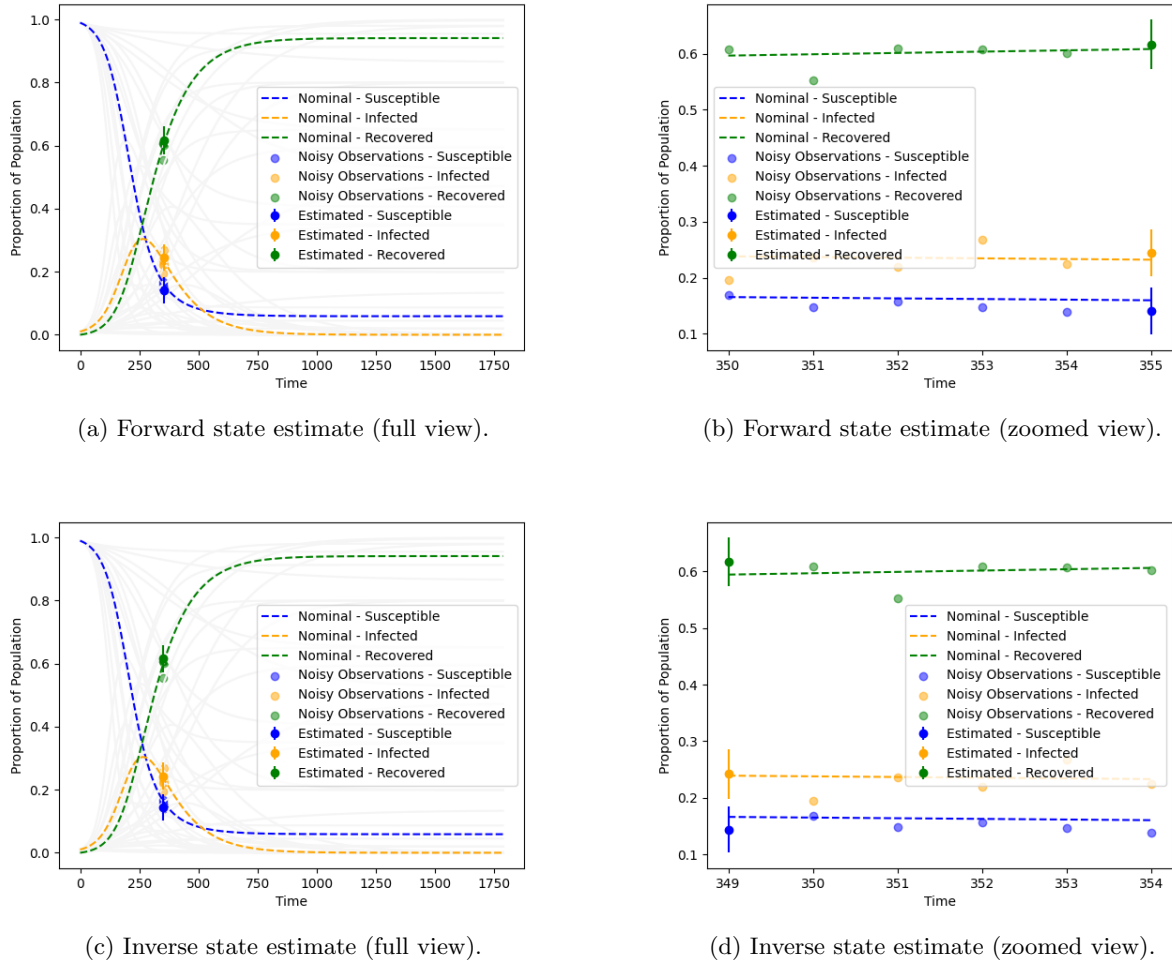


Figure 10: State estimates for normalizing flow conditioned on multiple trajectories using a transformer conditioning operator. Each row shows the full view (left) and a zoomed-in region (right). (a,b) Forward state estimates with noisy context. (c,d) Inverse state estimates with noisy context.

trajectories of the SIR systems that corresponds to the mean estimated parameters.

4 Discussion and Future Work

In this study, we consider a flexible family of NF-based approaches for online estimation of joint parameters and states that can easily combine information from physics or equation-based models, and observations from real processes. In particular, we evaluate the performance of different conditioning operators based on transformers and state-space model, respectively, and the effect of adding an optimal-transport-based kinetic energy loss term. Each method showed effectiveness for state estimation when applied to the autonomous driving dataset from Delecki et. al [23], with state-space models outperforming state-of-the-art transformers in some cases. The addition of a modified optimal transport-inspired kinetic loss term showed improved sampling efficiency by optimizing the probability path between each transformation in the flow. Expanding on the performance capability of the transformer conditioning operator, the optimal transport-inspired kinetic loss term provided similar capabilities in state estimation tasks, performing best in real COVID-19 case prediction.

In addition, we explore the application of our normalizing flow architecture in an epidemiological context.

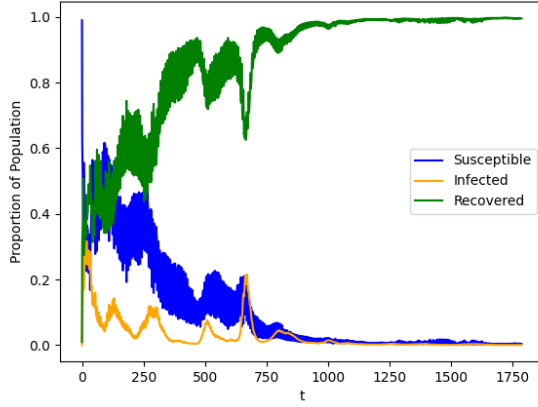


Figure 11: San Francisco COVID-19 SIR data.

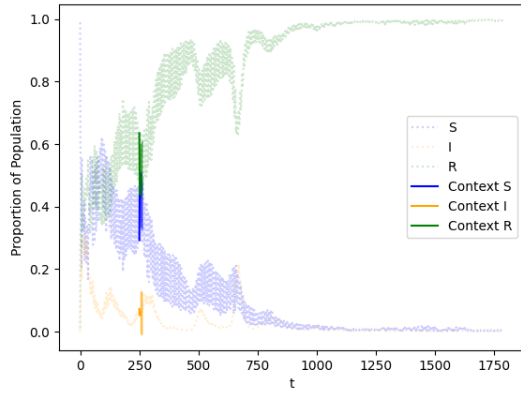
		Model								
		Transformer			Transformer + KE			Mamba-SSM		
Sample	fw	S	I	R	S	I	R	S	I	R
	bw	-0.178	-0.035	-0.175	0.113	0.810	0.256	0.970	1.274	2.075
	bw	-0.600	-0.068	-0.585	0.136	0.770	0.255	0.806	1.118	0.848

Table 4: Mean negative log likelihood of estimated conditional density given true observation. Forward and backward state estimation is performed at 100 randomly sampled locations along the San Francisco COVID-19 trajectory. The conditional NF predictor is trained on multiple SIR trajectories with various conditioning operators. Errors are shown separately for each compartment S , I , and R .

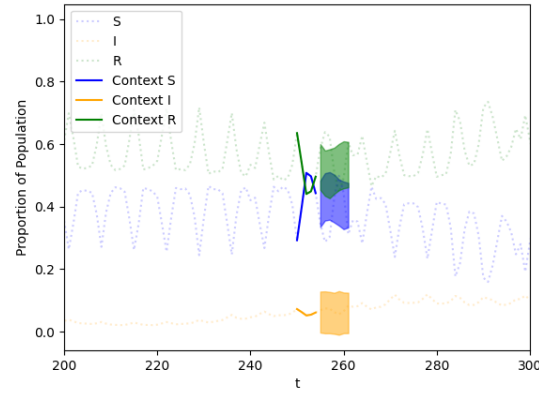
Mathematical models in their exact form, if at best, provide a highly generalized picture of a real-world system. That said, such dynamics, often developed by domain experts, contain important information about the reality of the underlying system. Operating under the assumption that the COVID-19 pandemic developed in a way somewhat described by the standard Susceptible-Infected-Recovered (SIR) model, we employ a conditional normalizing flow architecture to capture the underlying distribution in simulated noisy, multi-modal SIR trajectories and predict the next and previous states of real COVID-19 pandemic data. The expressivity of the conditional NF accurately models the noisy system of multiple SIR trajectories and showed high accuracy in forward and backward state predictions from a noisy context selected from one of the many simulated trajectories. Despite having only been trained on synthetic noisy data, conditional NF correctly captures forward and inverse trends in the real COVID-19 SIR data taken from the San Francisco Department of Public Health. Conditional NF maintained MAPE within the state-of-the-art range for COVID-19 forecasting with deep learning in some instances of one-week forecasting despite having not been exposed to any real data in training.

Conditional normalizing flows present a powerful method for capturing real-world system behavior that resembles an underlying mathematical model, combining deep learning methodology with domain expert research.

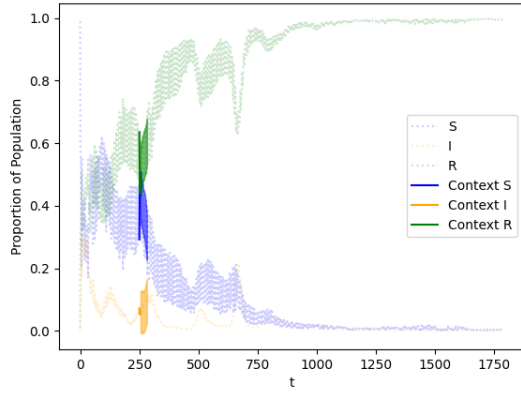
Furthermore, the flexibility of the architecture allowed for the addition of system parameters as targets in training, allowing for the prediction of such parameters given a context of states in time. This allows for a more practical understanding of the underlying system dynamics.



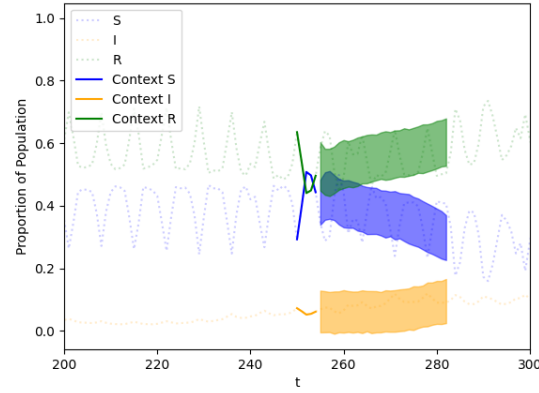
(a) 7-day window



(b) 7-day window (zoomed)



(c) 28-day window



(d) 28-day window (zoomed)

Figure 12: Forward rollout predictions of San Francisco COVID-19 data with 2σ error using a normalizing flow with transformer conditioning operator trained on multiple trajectories. Each row shows forward state estimation with different rolling window sizes: (a,b) 7-day and (c,d) 28-day.

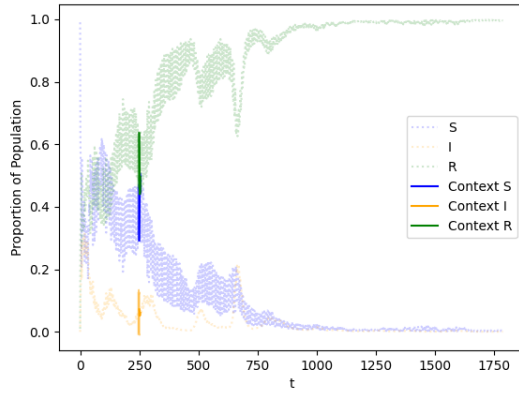
Future work will focus on further testing the efficacy in the joint prediction of states and parameters in more complex mathematical systems, and in fusing information from models with varying degree of fidelity and observations.

5 Acknowledgments

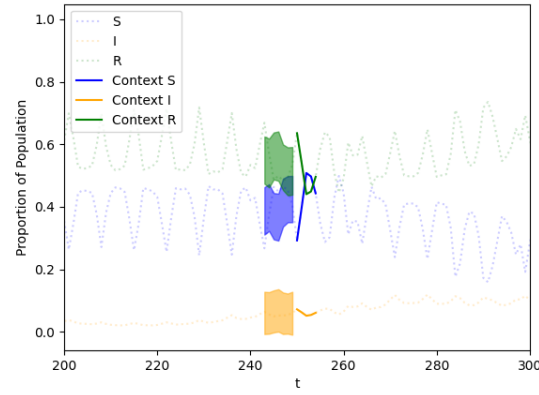
The authors acknowledge support from NSF CAREER award #1942662 (DES) and NSF CDS&E award #2104831 (DES), and from NIH grant #1R01HL167516. High performance computing resources for this study were provided by the Center for Research Computing at the University of Notre Dame.

References

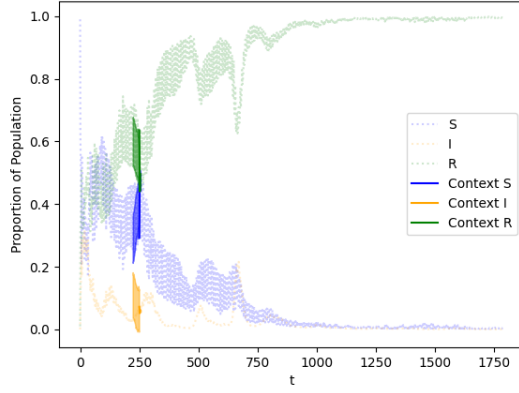
[1] R. E. Kalman. A new approach to linear filtering and prediction problems. *Journal of Basic Engineering*, 82(1):35–45, 03 1960.



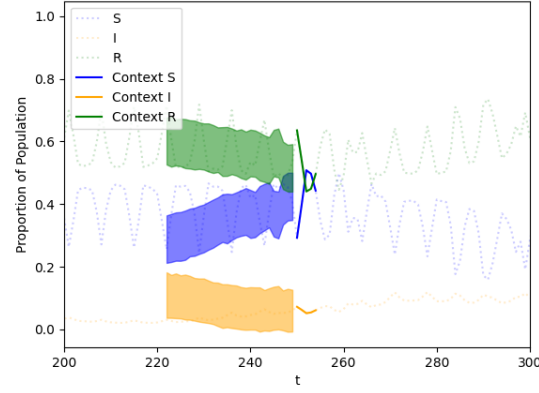
(a) 7-day window



(b) 7-day window (zoomed)



(c) 28-day window



(d) 28-day window (zoomed)

Figure 13: Backward rollout predictions of San Francisco COVID-19 data with 2σ error using a normalizing flow with transformer conditioning operator trained on multiple trajectories. Each row shows backward state estimation with different rolling window sizes: (a,b) 7-day and (c,d) 28-day.

- [2] Simon J. Julier and Jeffrey K. Uhlmann. New extension of the Kalman filter to nonlinear systems. In Ivan Kadar, editor, *Signal Processing, Sensor Fusion, and Target Recognition VI*, volume 3068, pages 182 – 193. International Society for Optics and Photonics, SPIE, 1997.
- [3] Bingbing Gao, Shesheng Gao, Yongmin Zhong, Gaoge Hu, and Chengfan Gu. Interacting multiple model estimation-based adaptive robust unscented Kalman filter. *International Journal of Control, Automation and Systems*, 15, 07 2017.
- [4] Thomas Bengtsson, Peter Bickel, and Bo Li. Curse-of-dimensionality revisited: Collapse of the particle filter in very large scale systems. In *Probability and statistics: Essays in honor of David A. Freedman*, volume 2, pages 316–335. Institute of Mathematical Statistics, 2008.
- [5] N. Vaswani. Particle filtering for large-dimensional state spaces with multimodal observation likelihoods. *IEEE Transactions on Signal Processing*, 56(10):4583–4597, October 2008.
- [6] Christopher M. Bishop. Mixture density networks. Workingpaper, Aston University, 1994.
- [7] Andreu Girbau, Xavier Giró i Nieto, Ignasi Rius, and Ferran Marqués. Multiple object tracking with mixture density networks for trajectory estimation, 2021.

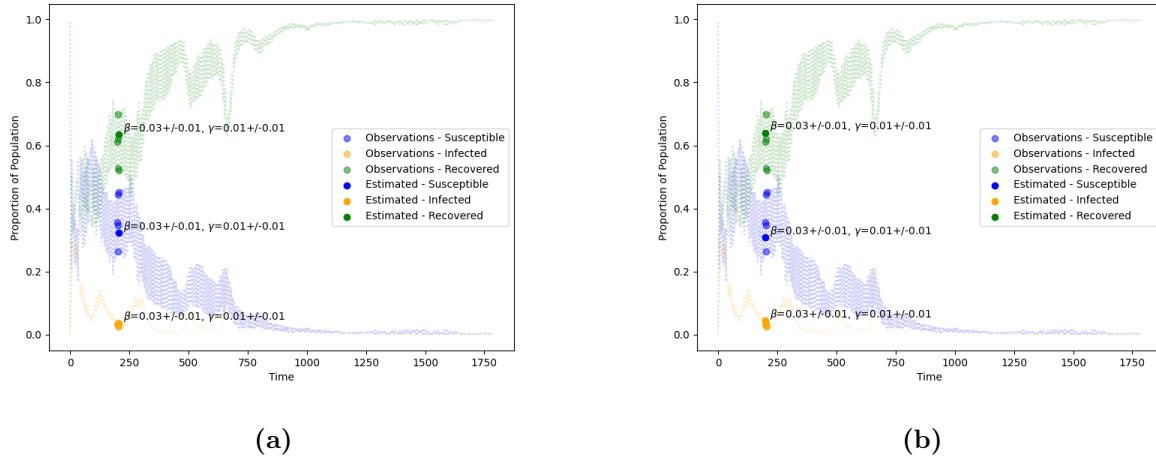


Figure 14: Joint state and parameter estimation using normalizing flow with transformer conditioning operator trained on multiple trajectories with San Francisco COVID-19 dataset. (a) Forward state estimation. (b) Inverse state estimation. We also add a visualization in gray for the SIR system’s trajectories that corresponds to the mean of the estimated parameters.

- [8] Xiaoming Li, Hubert Normandin-Taillon, Chun Wang, and Xiao Huang. XRMDN: An extended recurrent mixture density network for short-term probabilistic rider demand forecasting with high volatility, 2024.
- [9] Safa Messaoud, David A. Forsyth, and Alexander G. Schwing. Structural consistency and controllability for diverse colorization. *CoRR*, abs/1809.02129, 2018.
- [10] Moez Krichen. Generative adversarial networks. In *2023 14th International Conference on Computing Communication and Networking Technologies (ICCCNT)*, pages 1–7, 2023.
- [11] Diederik P Kingma and Max Welling. Auto-encoding variational Bayes, 2022.
- [12] Aman Singh and Tokunbo Ogunfunmi. An overview of variational autoencoders for source separation, finance, and bio-signal applications. *Entropy*, 24:55, 12 2021.
- [13] Tokunbo Ogunfunmi, Ravi Ramachandran, Roberto Togneri, Yuanjun Zhao, and Xianjun Xia. A primer on deep learning architectures and applications in speech processing. *Circuits, Systems, and Signal Processing*, 38, 08 2019.
- [14] Shaojie Chen, Zhaopeng Meng, and Qing Zhao. Electrocardiogram recognition based on variational autoencoder. In Jucheng Yang, Dong Sun Park, Sook Yoon, Yarui Chen, and Chuanlei Zhang, editors, *Machine Learning and Biometrics*, chapter 5. IntechOpen, Rijeka, 2018.
- [15] George Papamakarios, Eric Nalisnick, Danilo Jimenez Rezende, Shakir Mohamed, and Balaji Lakshminarayanan. Normalizing flows for probabilistic modeling and inference, 2021.
- [16] Jonathan Ho, Xi Chen, Aravind Srinivas, Yan Duan, and Pieter Abbeel. Flow++: Improving flow-based generative models with variational dequantization and architecture design, 2019.
- [17] Abdelrahman Abdelhamed, Marcus A. Brubaker, and Michael S. Brown. Noise flow: Noise modeling with conditional normalizing flows. In *Proceedings of the IEEE/CVF International Conference on Computer Vision (ICCV)*, October 2019.
- [18] Gurtej Kanwar, Michael S. Albergo, Denis Boyda, Kyle Cranmer, Daniel C. Hackett, Sébastien Racanière, Danilo Jimenez Rezende, and Phiala E. Shanahan. Equivariant flow-based sampling for lattice gauge theory. *Physical Review Letters*, 125(12), September 2020.

[19] Jonas Köhler, Leon Klein, and Frank Noé. Equivariant flows: sampling configurations for multi-body systems with symmetric energies, 2019.

[20] Frank Noé, Simon Olsson, Jonas Köhler, and Hao Wu. Boltzmann generators: Sampling equilibrium states of many-body systems with deep learning. *Science*, 365(6457):eaaw1147, 2019.

[21] Peter Wirnsberger, Andrew J. Ballard, George Papamakarios, Stuart Abercrombie, Sébastien Racanière, Alexander Pritzel, Danilo Jimenez Rezende, and Charles Blundell. Targeted free energy estimation via learned mappings. *The Journal of Chemical Physics*, 153(14), October 2020.

[22] Xuechen Li, Ting-Kam Leonard Wong, Ricky T. Q. Chen, and David Duvenaud. Scalable gradients for stochastic differential equations, 2020.

[23] Harrison Delecki, Liam A. Kruse, Marc R. Schlichting, and Mykel J. Kochenderfer. Deep normalizing flows for state estimation, 2023.

[24] Ivan Kobyzev, Simon JD Prince, and Marcus A Brubaker. Normalizing flows: An introduction and review of current methods. *IEEE transactions on pattern analysis and machine intelligence*, 43(11):3964–3979, 2020.

[25] Laurent Dinh, Jascha Sohl-Dickstein, and Samy Bengio. Density estimation using real NVP. *arXiv preprint arXiv:1605.08803*, 2016.

[26] George Papamakarios, Theo Pavlakou, and Iain Murray. Masked autoregressive flow for density estimation. *Advances in neural information processing systems*, 30, 2017.

[27] Conor Durkan, Artur Bekasov, Iain Murray, and George Papamakarios. nflows: normalizing flows in PyTorch, November 2020.

[28] Neo Wu, Bradley Green, Xue Ben, and Shawn O’Banion. Deep transformer models for time series forecasting: The influenza prevalence case, 2020.

[29] Ken C Pohlmann. *Principles of digital audio*. McGraw-Hill Professional, 2000.

[30] Albert Gu and Tri Dao. Mamba: Linear-time sequence modeling with selective state spaces, 2024.

[31] Cédric Villani. *Topics in optimal transportation*, volume 58. American Mathematical Soc., 2021.

[32] Neta Shaul, Ricky T. Q. Chen, Maximilian Nickel, Matt Le, and Yaron Lipman. On kinetic optimal probability paths for generative models, 2023.

[33] Han Huang, Jiajia Yu, Jie Chen, and Rongjie Lai. Bridging mean-field games and normalizing flows with trajectory regularization. *Journal of Computational Physics*, 487:112155, 2023.

[34] F. Pedregosa, G. Varoquaux, A. Gramfort, V. Michel, B. Thirion, O. Grisel, M. Blondel, P. Prettenhofer, R. Weiss, V. Dubourg, J. Vanderplas, A. Passos, D. Cournapeau, M. Brucher, M. Perrot, and E. Duchesnay. Scikit-learn: Machine Learning in Python. *Journal of Machine Learning Research*, 12:2825–2830, 2011.

[35] Fernando Pérez-Cruz. Kullback-Leibler divergence estimation of continuous distributions. In *2008 IEEE international symposium on information theory*, pages 1666–1670. IEEE, 2008.

[36] San Francisco Department Health. COVID-19 data and reports. <https://www.sf.gov/resource--2021--covid-19-data-and-reports>. [Accessed 25-02-2025].

[37] Hadeel AlQadi and Majid Bani-Yaghoub. Incorporating global dynamics to improve the accuracy of disease models: Example of a COVID-19 SIR model. *PLoS One*, 17(4):e0265815, April 2022.